

# Elastically driven anisotropic percolation in electronic phase-separated manganites

T. Z. Ward<sup>1</sup>, J. D. Budai<sup>1</sup>, Z. Gai<sup>1,2</sup>, J. Z. Tischler<sup>1</sup>, Lifeng Yin<sup>1</sup> and J. Shen<sup>1,3\*</sup>

**The presence of electronic phase separation in complex materials has been linked to many types of exotic behaviour, such as colossal magnetoresistance, the metal–insulator transition and high-temperature superconductivity<sup>1–4</sup>; however, the mechanisms that drive the formation of coexisting electronic phases are still debated<sup>5–8</sup>. Here we report transport measurements that show a preferential orientation of electronic phase domains driven by anisotropic long-range elastic coupling between a complex oxide film and substrate. We induce anisotropic electronic-domain formation along one axis of a pseudocubic perovskite single-crystal thin-film manganite by epitaxially locking it to an orthorhombic substrate. Simultaneous temperature-dependent resistivity measurements along the two perpendicular in-plane axes show substantial differences in the metal–insulator transition temperature and extraordinarily high anisotropic resistivities, which indicate that percolative conduction channels open more readily along one axis. These findings suggest that the origin of phase coexistence is much more strongly influenced by strain than by local chemical inhomogeneity.**

Complex oxides have a wide range of unique behaviours owing to their often inseparable energy overlaps of the spin–charge–lattice–orbital interactions. Manganites are of particular interest owing to the speculation that their colossal-magnetoresistive behaviour is the result of emergent electronic phase separation (EPS). In the EPS model, coexisting regions with drastically different electronic properties can form into domains of the order of nanometres to micrometres in single-crystal structures. There is a great deal of debate about the mechanisms that cause EPS. At present, many theories cite local chemical disorder or complex electronic interactions as the key mechanisms<sup>5–8</sup>; however, the influence of inherent crystalline strain and local lattice distortions are also thought to have a strong influence over the formation of EPS (refs 9–13). Combining these influences, theoretical models based on electronic and elastic degrees of freedom have shown that large-scale EPS can self-organize into elongated domains with no preference for uniaxial orientation<sup>9</sup>. By applying an anisotropic long-range strain field to an EPS system, we can investigate the specific effects of elastic energy on the emergent formation of coexisting electronic phase domains. Owing to its well-known large-scale EPS into ferromagnetic-metal (FMM) and charge-ordered-insulator (COI) domains, we use single-crystal thin films of  $\text{La}_{5/8-x}\text{Pr}_x\text{Ca}_{3/8}\text{MnO}_3$  ( $x = 0.3$ ) (LPCMO) as a model system and compare the transport data of two perpendicular in-plane directions in the case of an anisotropically strained orthorhombic structure. Although other methods, such as magnetic force microscopy<sup>14–16</sup> and out-of-plane versus in-plane transport<sup>17</sup>, have found evidence of local variation in domain

formation owing to strain effects, the ability of in-plane anisotropic transport measurements to identify the percolation point in metal–insulator transitions (MITs) on global levels make this the ideal method for understanding how emergent EPS affects macroscopic properties such as colossal magnetoresistance and the metal–insulator transition.

Although bulk LPCMO is a pseudo-cubic perovskite at room temperature<sup>18</sup>, it is possible to force a thin film to epitaxially conform to the in-plane lattice parameters of a closely matched substrate. Figure 1a shows X-ray diffraction measurements of the temperature-dependent lattice spacings for a 50-nm-thick LPCMO film that is lattice locked to an orthorhombic  $\text{NdGaO}_3$  (NGO) substrate. In-plane lattice commensurability induces anisotropic, tensile strain fields in the epitaxial film—showing a tensile strain of 0.003 and 0.001 in the in-plane directions. The inset gives a representation of the film and (101) substrate with their appropriate lattice directions labelled. For simplicity, we will discuss strain and transport directions in terms of the LPCMO film indices using the orthorhombic  $Pnma$  convention—where the long axis is labelled  $b$ . This strain is present throughout the cooling process, with the film and substrate being commensurate across the entire temperature region from 300 to 34 K (Fig. 1b). Figure 1b is a mesh scan in reciprocal space, where the vertical axis corresponds to the out-of-plane direction and the two peaks show the commensurability of the substrate and LPCMO film. The weaker finite-thickness peaks observed in the mesh scan are shown over a larger range in the  $\theta$ – $2\theta$  scan in Fig. 1c, and the presence of many smaller internal interference peaks further confirms the uniformity and epitaxy of the film.

If strain fields drive the formation of EPS, transport responses in a single sample should show variations dependent on the measurement's relation to the underlying strain. We find this to be the case for the 50-nm-thick LPCMO film on NGO, where epitaxy drives the anisotropic strain field (Fig. 2a). Transport is shown along the two in-plane directions corresponding to the  $[10\bar{1}]$  and  $[101]$  directions (Fig. 2b inset). Remarkably, the MIT temperature ( $T_{\text{MIT}}$ ) measured along the higher-strained  $[10\bar{1}]$  direction is 24 K higher than that measured along the  $[101]$  direction. The difference between the resistivities measured at the respective  $T_{\text{MIT}}$  values is  $0.31 \Omega \text{ cm}$ , which corresponds to a relative variation of  $\sim 200\%$ . In fact, the anisotropic resistivity,  $m$  that is, relative difference in resistivities compared at the same temperature  $((\rho_{[101]} - \rho_{[10\bar{1}]})/\rho_{[10\bar{1}]})$ — $m$  is even larger, reaching 500% at 110 K (Fig. 2b). Interestingly, in the temperature range between the two  $T_{\text{MIT}}$  values, the system acts as a metal in the  $[10\bar{1}]$  direction and an insulator in the  $[101]$  direction.

To verify that these striking behaviours are indeed induced by the anisotropic strain field, we made transport measurements on

<sup>1</sup>Materials Sciences and Technology Division, Oak Ridge National Laboratory, Oak Ridge, Tennessee 37830, USA, <sup>2</sup>Center for Nanophase Materials Sciences Division, Oak Ridge National Laboratory, Oak Ridge, Tennessee 37830, USA, <sup>3</sup>Department of Physics and Astronomy, The University of Tennessee, Knoxville, Tennessee 37996, USA. \*e-mail: shenj@ornl.gov.

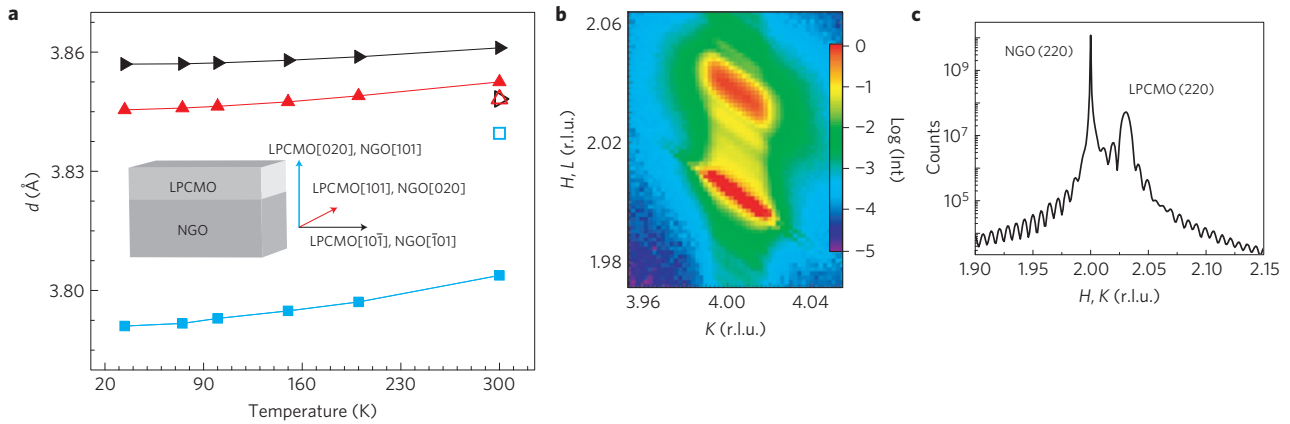


**Figure 1 | Lattice configuration.** **a**, NdGaO<sub>3</sub> (NGO) substrate acts to lock a 50 nm La<sub>5/8-x</sub>Pr<sub>x</sub>Ca<sub>3/8</sub>MnO<sub>3</sub> (LPCMO) epitaxial film (closed symbols) into an in-plane anisotropic strained state that is not possible in bulk LPCMO (open symbols)<sup>18</sup>. (Inset) Diagram of notation showing lattice alignment in *Pnma* notation for NGO and LPCMO, with arrow colours corresponding to the directions in **a**. **b**, Typical reciprocal-space mesh scan taken at 120 K showing that LPCMO film is commensurate with NGO substrate. **c**,  $\theta-2\theta$  scan demonstrating the quality of the film. (See Supplementary Methods.)

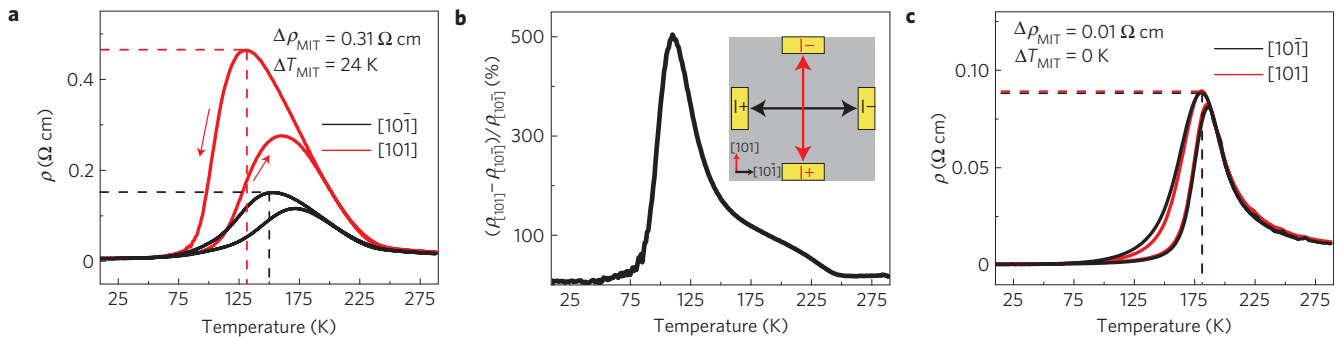


**Figure 2 | In-plane transport properties.** **a**, LPCMO film on an NGO substrate has anisotropic in-plane strain and shows significant differences in both the MIT temperature and the resistivity at the MIT depending on MIT along which axis transport is taken across. Arrows indicate cooling and warming curves taken under a 7.5 T magnetic field. **b**, Relative percentage difference between cooling curves along perpendicular in-plane directions for LPCMO on NGO. (Inset) Diagram showing directions of transport in the LPCMO thin film relative to the in-plane axes. **c**, LPCMO film on an SLGO substrate has isotropic in-plane strain and shows negligible differences in transport along the two in-plane axes. Note that for **c** strain field along [101] = strain field along  $[10\bar{1}]$  whereas in **a** strain field along [101] < strain field along  $[10\bar{1}]$ . (See Supplementary Methods.)

a 50 nm LPCMO film grown on a SrLaGaO<sub>4</sub> (SLGO) substrate, which is tetragonal with in-plane lattice parameters of equal value of less than 0.1% difference from bulk LPCMO (refs 18, 19). Figure 2c shows the temperature-dependent resistivity for the LPCMO film that is in-plane lattice locked to the SLGO(001) substrate. Comparing the in-plane transport curves, we see that there is a relative variation of only ~1% in the resistivity at the MIT and that there is no difference in  $T_{\text{MIT}}$ . These measurements were conducted under no applied magnetic field to maximize any anisotropic resistive differences that might be present; indeed, increasing the applied magnetic field to 3 T reduces the difference in resistivities at the MIT to nearly zero (not shown). Note that the SLGO and the NGO substrates used for these measurements have very small miscut angles of ~0.1° along the [101] direction. On the basis of the transport data from the LPCMO/SLGO thin film, it seems that the miscut has a negligible effect on anisotropy of transport. This strongly suggests that the anisotropic strain field applied by the NGO substrate must be the driving mechanism for the observed differences.

Because the MIT in the LPCMO system is percolative in nature<sup>10,16</sup>, the higher  $T_{\text{MIT}}$  along the strained  $[10\bar{1}]$  direction indicates that there is a preferential seeding and growth of ferromagnetic metallic domains along the  $[10\bar{1}]$  direction. If this is indeed the case, we would expect that the easy magnetization axis is aligned along the  $[10\bar{1}]$  direction. Figure 3a shows magnetization

measurements along each of the two in-plane directions. Clearly, the susceptibility is considerably higher in the strained  $[10\bar{1}]$  direction than in the [101] direction. This is consistent with the scenario in which the FMM phase domains have an elongated aspect ratio, which develops along the direction of the greater strain field.

Figure 3b presents an illustration of how elongated domains act to channel current. Percolative models developed to describe fluid flow through elongated channels have been suitably studied and have shown that transport occurs most easily along the elongated direction<sup>20-22</sup>. In the LPCMO case, the easier percolation means a higher  $T_{\text{MIT}}$ . Between the current contacts, the electrons travel along the path of least resistance. In an insulating background with preferentially elongated metallic domains oriented along one direction, the measured resistivity in line with the metallic domains will be substantially lower. This is because the transport channel will not be forced to travel across as much of the insulating region when there are available metallic regions. This explains the large anisotropic resistivity observed in the system.

Further, in the case of the insulating background being COI, the application of a magnetic field would effectively melt the insulating phase into a metallic phase and destroy the anisotropic nature of the transport<sup>23,24</sup>. Figure 3c shows  $T_{\text{MIT}}$  for both the  $[10\bar{1}]$  and the [101] directions as a function of magnetic field. At all magnetic fields, the direction with the highest strain field, that is, the  $[10\bar{1}]$  direction, has a consistently lower  $T_{\text{MIT}}$  value.

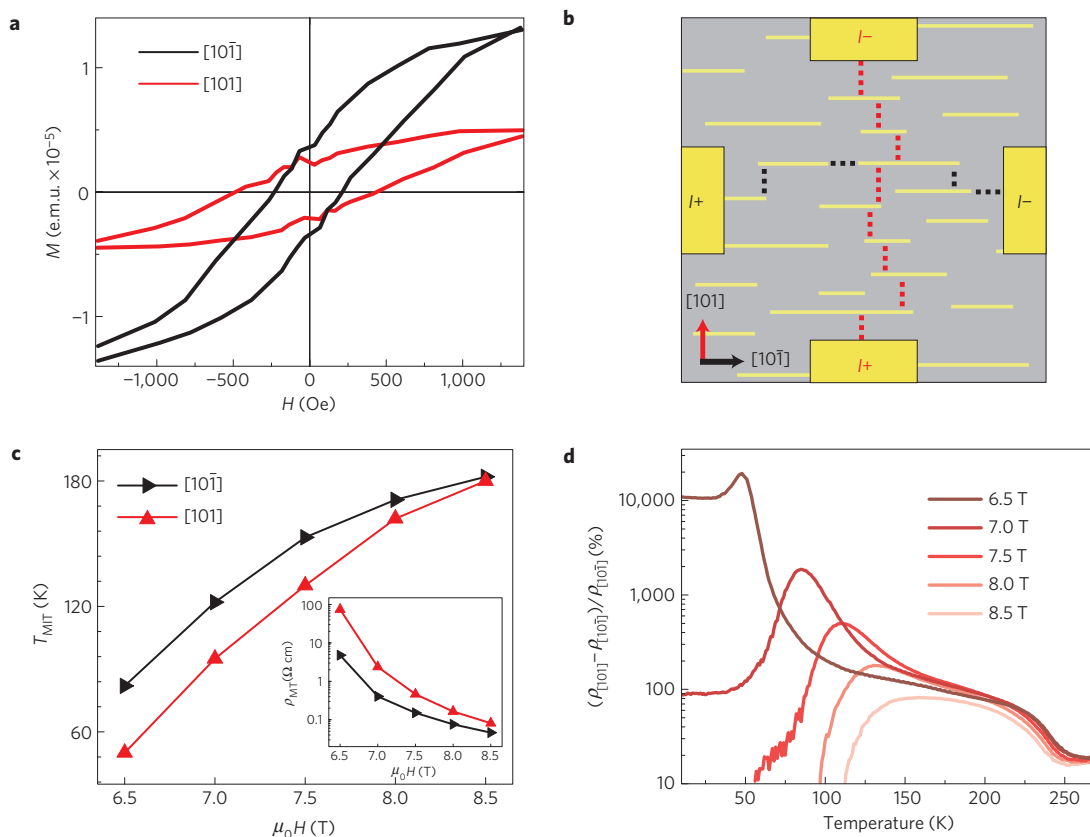


**Figure 3 | Effects of anisotropic strain field applied through NGO substrate on LPCMO film.** **a**, Magnetization ( $M$ ) data at 120 K with magnetic field ( $H$ ) applied along each of the in-plane directions shows that the easy axis is along the  $[10\bar{1}]$  direction. **b**, Diagram of a percolative model in which the metallic phase domains have an elongated aspect ratio directed along the axis under the higher strain field. Yellow lines indicate randomly seeded regions of low resistance laid in a high-resistance background. Dotted lines indicate possible high-resistance channels through which current must travel in each direction. **c**, With increasing magnetic field, the anisotropy seen in the MIT temperature along each in-plane axis decreases. (Inset) The anisotropy in the resistivity at the MIT along each in-plane axis decreases with increased field. **d**, Resistivity percentage difference between orthogonal in-plane cooling curves is maximized at low field. (See Supplementary Methods.)

By increasing the applied magnetic field, the MIT temperatures converge. For example, the difference in the  $T_{\text{MIT}}$  shrinks from 32 K at 6.5 T to a mere 1 K at 8.5 T. This can be understood because at 8.5 T the applied field is sufficient to counteract the effects of preferential domain formation caused by the anisotropic strain field and the transition temperatures become nearly identical. This effect can also be seen in the resistivities at the respective MIT points along each direction (Fig. 3c inset); as the metallic channels equalize at 8.5 T, the difference in resistivity along the two directions approaches zero. The field-dependent anisotropic transport behaviour is, therefore, again consistent with a percolative transport network in which there is a preference in aspect ratio of FMM domain formation in a COI background.

Finally, we note that the anisotropic resistivity is extraordinarily high in this system (Fig. 3d). For instance, the anisotropy resistivity reaches  $\sim 20,000\%$  at 48 K under a 6.5 T field. With increased magnetic field, this difference is reduced. As discussed above, the melting of the COI phase destroys the elongated aspect ratio of the metallic domains, which means that the current path along the  $[101]$  direction is no longer as dominated by the insulating regions. This behaviour also allows for magnetic-field-tunable anisotropic resistivity.

The large anisotropic transport behaviour of the LPCMO system under the presence of an anisotropic strain field indicates that the formation of EPS depends sensitively on long-range elastic strain. We have shown that the formation and orientation of EPS domains can be guided by applying a uniaxial strain field. Even within the

same plane, the metallicity can change drastically along different directions with respect to that of the strain field. Consequently, the system shows extraordinarily large anisotropic resistivity, which can, in turn, be used to detect subtle changes in the external strain field from the environment. These findings show that emergent electronic-phase-domain formation can be selectively tuned over long distances, which opens the door to new device engineering and a fuller understanding of the balanced energetics that drive emergent behaviours in complex materials.

Received 13 May 2009; accepted 28 August 2009;  
published online 4 October 2009

## References

- Dagotto, E., Hotta, T. & Moreo, A. Colossal magnetoresistant materials: The key role of phase separation. *Phys. Reports* **344**, 1–3 (2001).
- Shenoy, V. B., Sarma, D. D. & Rao, C. N. R. Electronic phase separation in correlated oxides: The phenomenon, its present status and future prospects. *Chem. Phys. Chem.* **7**, 2053–2059 (2006).
- Mathur, N. D. & Littlewood, P. B. The self-organised phases of manganites. *Solid State Commun.* **119**, 271–280 (2001).
- Cox, S. *et al.* Sliding charge-density wave in manganites. *Nature Mater.* **7**, 25–30 (2008).
- Milward, G. C., Calderón, M. J. & Littlewood, P. B. Electronically soft phases in manganites. *Nature* **433**, 607–610 (2005).
- Ghivelder, L. & Parisi, F. Dynamic phase separation in  $\text{La}_{5/8-y}\text{Pr}_y\text{Ca}_{3/8}\text{MnO}_3$ . *Phys. Rev. B* **71**, 184425 (2005).
- Burgy, J., Moreo, A. & Dagotto, E. Relevance of cooperative lattice effects and stress fields in phase-separation theories for CMR manganites. *Phys. Rev. Lett.* **92**, 097202 (2004).

8. Salamon, M. B. & Jaime, M. The physics of manganites: Structure and transport. *Rev. Mod. Phys.* **73**, 583–628 (2001).
9. Ahn, K. H., Lookman, T. & Bishop, A. R. Strain-induced metal–insulator phase coexistence in perovskite manganites. *Nature* **428**, 401–404 (2004).
10. Uehara, M. *et al.* Percolative phase separation underlies colossal magnetoresistance in mixed-valent manganites. *Nature* **399**, 560–563 (1999).
11. Ward, T. Z. *et al.* Reemergent metal–insulator transitions in manganites exposed with spatial confinement. *Phys. Rev. Lett.* **100**, 247204 (2008).
12. Gillaspie, D. *et al.* Influence of different substrates on phase separation in  $\text{La}_{1-x-y}\text{Pr}_y\text{Ca}_x\text{MnO}_3$  thin films. *J. Appl. Phys.* **99**, 08S901 (2006).
13. Dhakal, T., Tosado, J. & Biswas, A. Effect of strain and electric field on the electronic soft matter in manganite thin films. *Phys. Rev. B* **75**, 092404 (2007).
14. Wu, W. *et al.* Magnetic imaging of a supercooling glass transition in a weakly disordered ferromagnet. *Nature Mater.* **5**, 881–886 (2006).
15. Dho, J. *et al.* Strain-induced magnetic stripe domains in  $\text{La}_{0.7}\text{Sr}_{0.3}\text{MnO}_3$  thin films. *Appl. Phys. Lett.* **82**, 1434–1436 (2003).
16. Zhang, L. *et al.* Direct observation of percolation in a manganite thin film. *Science* **298**, 805–807 (2002).
17. Rairigh, R. P. *et al.* Colossal magnetocapacitance and scale-invariant dielectric response in phase-separated manganites. *Nature Phys.* **3**, 551–555 (2007).
18. Inorganic crystal structure database, <<http://www.fiz-karlsruhe.de/fiz/products/icsd/icsd.html>>. (FIZ Karlsruhe, 2008).
19. Drozdowski, M. *et al.* Temperature study of lattice constants and Raman scattering of  $\text{SrLaGaO}_4$  single crystal. *Solid State Commun.* **96**, 785–788 (1995).
20. Barthélémy, J. Effective permeability of media with a dense network of long and micro fractures. *Transp. Porous Media* **76**, 153–178 (2009).
21. Gueguen, Y. & Dienes, J. Transport properties of rocks from statistics and percolation. *Math. Geol.* **21**, 1–13 (1989).
22. Philip, Z. *et al.* Modeling coupled fracture-matrix fluid flow in geomechanically simulated fracture networks. *SPE Reservoir Eval. Eng.* **8**, 300–309 (2005).
23. Macia, F. *et al.* Observation of phonon-induced magnetic deflagration in manganites. *Phys. Rev. B* **76**, 174424 (2007).
24. Tomioka, Y. *et al.* Collapse of a charge-ordered state under a magnetic field in  $\text{Pr}_{1/2}\text{Sr}_{1/2}\text{MnO}_3$ . *Phys. Rev. Lett.* **74**, 5108–5111 (1995).

### Acknowledgements

This effort was supported by the US DOE Office of Basic Energy Sciences, Division of Materials Science and Engineering, through the Oak Ridge National Laboratory. Research was carried out by T.Z.W. as a Eugene P. Wigner Fellow and staff member at Oak Ridge National Laboratory, under contract DE-AC05-00OR22725. A portion of this research at ORNL's CNMS was sponsored by the Scientific User Facilities Division, Office of ES, US DOE. The use of the APS was supported by the US DOE, Office of Science, Office of Basic Energy Sciences. We thank J. Karapetrova for set-up help at APS beamline XOR/UNI.

### Author contributions

T.Z.W., J.D.B. and J.S. conceived and designed the experiment. T.Z.W. grew samples and carried out transport experiments. J.D.B. and J.Z.T. carried out synchrotron experiments. Z.G. and L.Y. carried out magnetization experiments. T.Z.W., J.D.B. and J.S. analysed data and wrote the paper.

### Additional information

Supplementary information accompanies this paper on [www.nature.com/naturephysics](http://www.nature.com/naturephysics). Reprints and permissions information is available online at <http://npg.nature.com/reprintsandpermissions>. Correspondence and requests for materials should be addressed to J.S.